Developmental Cell *18*

Supplemental Information

Kinetochores Generate Microtubules with Distal Plus Ends: Their Roles and Limited Lifetime in Mitosis

Etsushi Kitamura, Kozo Tanaka, Shinya Komoto, Yoko Kitamura, Claude Antony, and Tomoyuki U. Tanaka

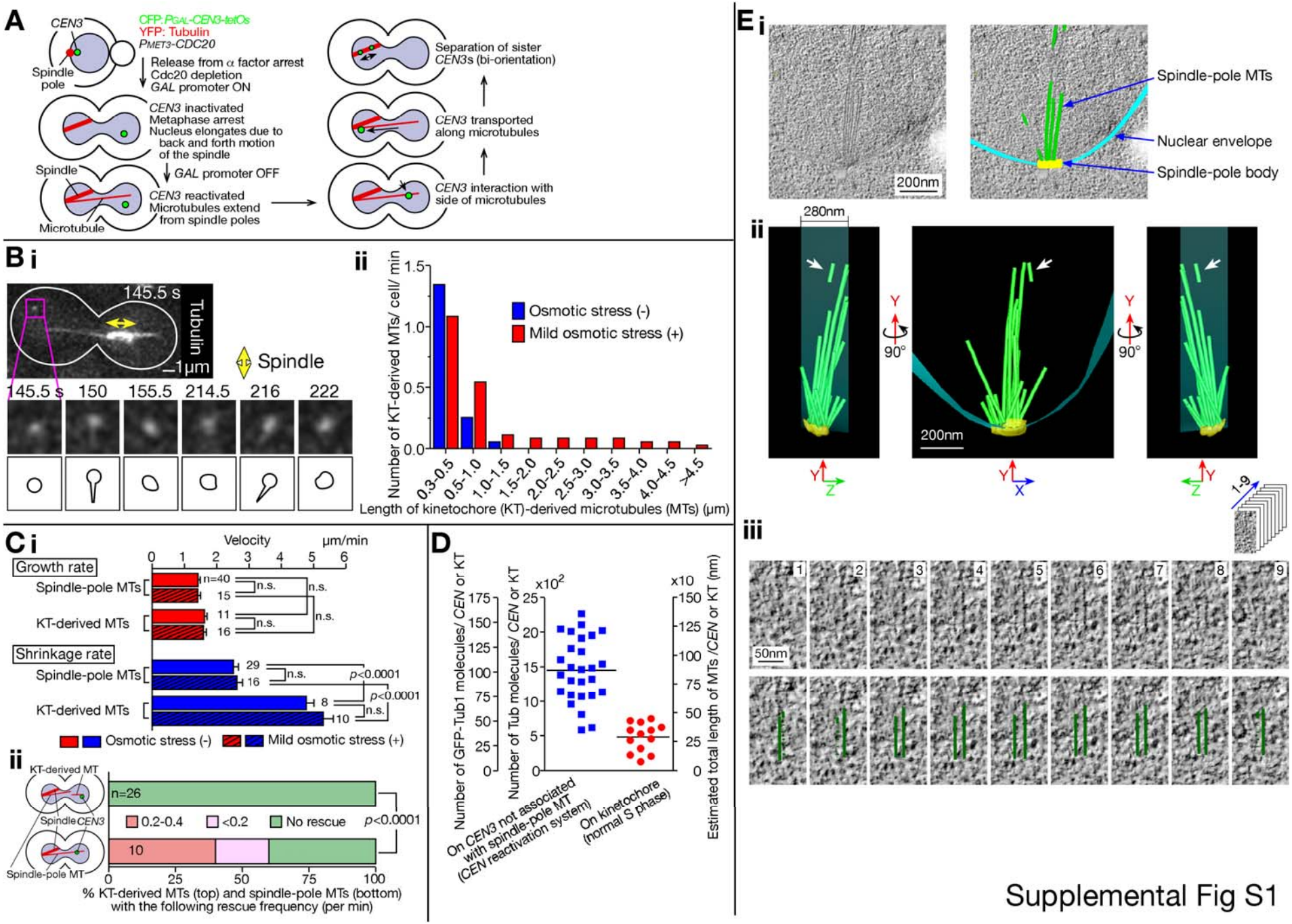

Supplemental Fig S1

Figure S1, (associated with Figure 1).

(A) Schematic drawing of a *CEN* reactivation assay

Using this assay, we can displace a centromere further away from a spindle pole. See detail in main text and in Tanaka et al., 2005.

(B) Microtubules extend from kinetochores prior to their interaction with spindle-pole microtubules

(i) Short microtubules often extend from kinetochores in most of the cells in the absence of mild osmotic stress. *PGAL-CEN3-tetOs GFP-TUB1 PMET3-CDC20* cells (T7673) were treated as in Fig 1B (note that an array of *tetO*s was not visualized in this strain). GFP (tubulin) images were acquired every 1.5 sec for 10 min. Representative time-lapse images (top) with schematic diagrams (bottom) show extension of short (about 500 nm) microtubules from the *CEN3*-associated punctate GFP Tub1 signal. *Results*: We often observed a punctate GFP signal apart from the spindle and the majority of such GFP signal subsequently interacted with spindle-pole microtubules. We interpreted that the GFP signal was associated with *CEN3*.

(ii) Distribution of the maximum extension of kinetochore (KT)-derived microtubules (MTs) in the absence (blue bars) and presence (red bars) of osmotic shock. *PGAL-CEN3-tetOs TetR-4×mCherry GFP-TUB1 PMET3-CDC20* cells (T7715) were treated as in Fig 1B and Fig 1C, respectively. GFP (tubulin) images were acquired every 2 sec. At the start of imaging, mCherry images were also acquired in order to confirm that GFP signals were associated with mCherry signals (i.e. *CEN3*). In each condition, 7 cells were analyzed for 5 min. Each bar shows the average number of microtubules (per cell per min) with the categorized length at maximum extension.

(C) Dynamics of kinetochore-derived microtubules: comparison with spindle-pole microtubules

(i) Growth and shrinkage rate. T3828 cells (see Fig 1B) were treated as in Fig 1B (with no osmotic stress) and in Fig 1C (with mild osmotic stress: striped), and images were acquired every 30 sec as in Fig 1C. Graphs show the growth rate (red) and shrinkage rate (blue) of spindle-pole microtubules with no *CEN3* attached, and of kinetochore-derived microtubules. n: number of observed events. Error bars show SEM. n.s.: not significant.

(ii) Kinetochore-derived microtubules did not show microtubule rescue, in contrast to spindle-pole microtubules that were associated with *CEN3*. T6718 cells (see Fig 5B) were treated as in Fig 1C. mCherry (Bik1; green), YFP (tubulin; red), and CFP (*CEN3*; blue) images were acquired every 20 sec for 25 min. The frequency of microtubule rescue (per min) was categorized as shown in the graph. For spindle-pole microtubules, only those that were associated with *CEN3* were taken into consideration. n: number of observed microtubules.

(D) Quantifying the number of tubulin molecules localizing at kinetochores

In normal S phase and in the centromere reactivation system, the intensity of punctate GFP-Tub1 signals, associated with KTs, was compared with that of Cse4-GFP. Cse4 is a histone H3 variant at a centromere and 32 molecules (2 molecules per centromere; Furuyama and Biggins, 2007) should be present close to a single spindle pole where 16 centromeres are clustered in telophase. From this comparison, we estimated how many GFP-Tub1 molecules were present at each kinetochore.

(E) Short microtubules, not connected to an SPB, are found during S phase using electron tomography

Wild-type cells (K699, W303 background) were treated with α-factor and subsequently released to fresh media. After 20-30 min, cells were collected and frozen under high pressure. The samples were then freeze-substituted, embedded, cut into sections and post-stained. Tilt series of electron micrographs were acquired and reconstituted to 3D tomograms.

(i) A representative electron micrograph (left) showing an SPB, spindle-pole microtubules and the nuclear envelope (coloured in right).

(ii) 3D reconstitution of image series of the example shown in (i). A presumptive short microtubule (white arrow) was not connected to an SPB as its both ends were within the 280 nm section (see images at left and right).

(iii) A series of electron micrographs of the presumptive short microtubule, indicated by a white arrow in (ii). Its edges are shown in green lines at bottom. Note that its top end seems to have a sheet-like structure as its right-hand edge extends longer than its left.

Results: Electron tomography analysis identified structures that seemed to be short microtubules, which were not connected to a spindle pole, during early S phase when kinetochores, not associated with spindle-pole microtubules were present (see Fig 1A; Fig 6A, B); these microtubules may originate from kinetochores. However the positions of kinetochores could not be determined with this method, as the electron beam does not produce sufficient contrast to visualise yeast kinetochores (O'Toole et al., 1999).

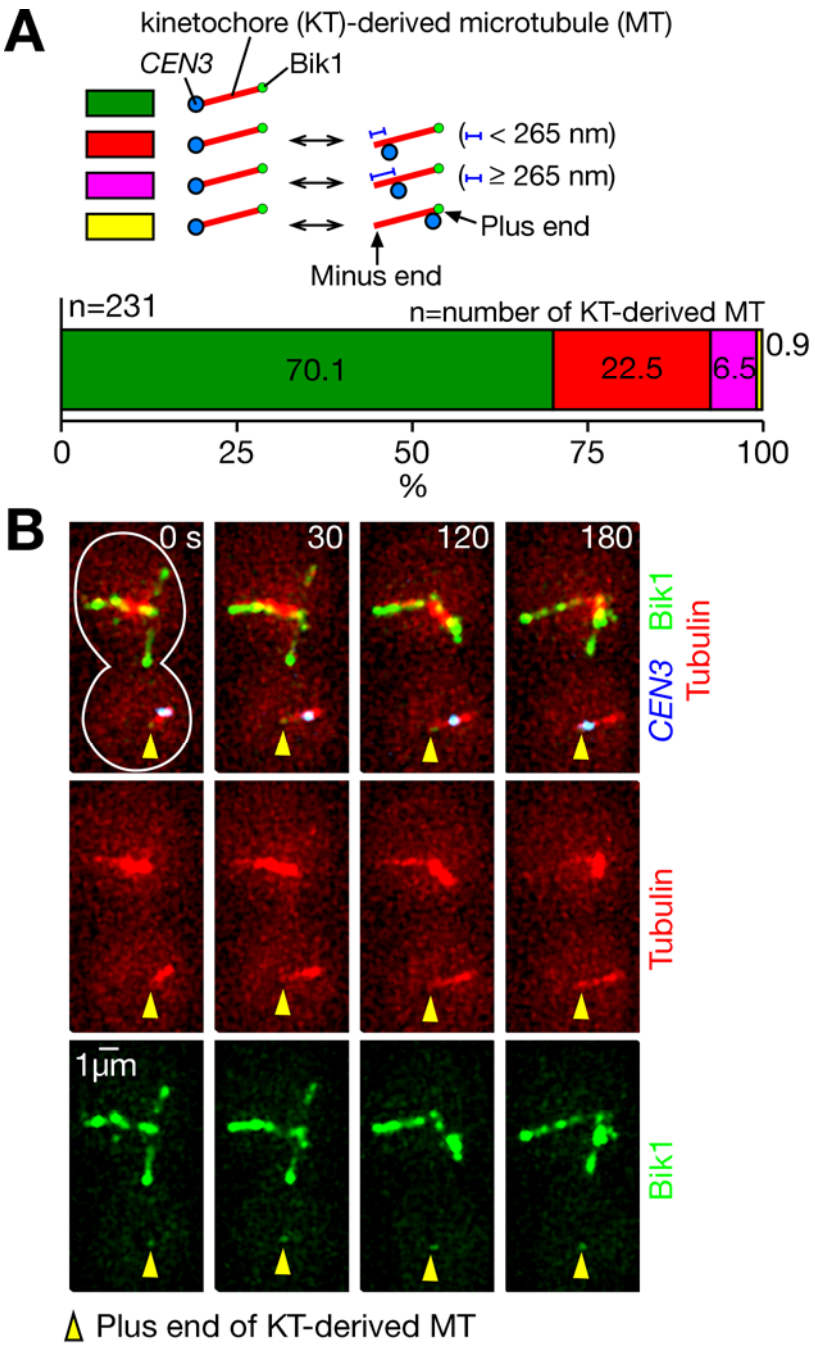

Supplemental Fig S2

Figure S2, (associated with Figure 2). After *CEN3* has nucleated microtubules, it occasionally leaves their minus ends and moves along their lateral surface

PGAL-CEN3-tetOs TetR-3xCFP YFP-TUB1 BIK1-4xmCherry PMET3-CDC20 cells (T6718) were treated as in Fig 1C. mCherry (Bik1; green), YFP (tubulin; red), and CFP (*CEN3*; blue) images were acquired every 30 sec for 25 min.

(A) Percentages of cells in which *CEN3* migrated to the lateral side of the microtubule that had been originally extended from *CEN3*. Cells were classified according to the maximum distance from the minus end, which *CEN3* had reached.

(B) A time-lapse image sequence, in which *CEN3* had reached the vicinity of the plus-end of a *CEN3*-derived microtubule (rare event: see A). Zero time is set arbitrarily for the first panel, in which a cell shape is outlined in white.

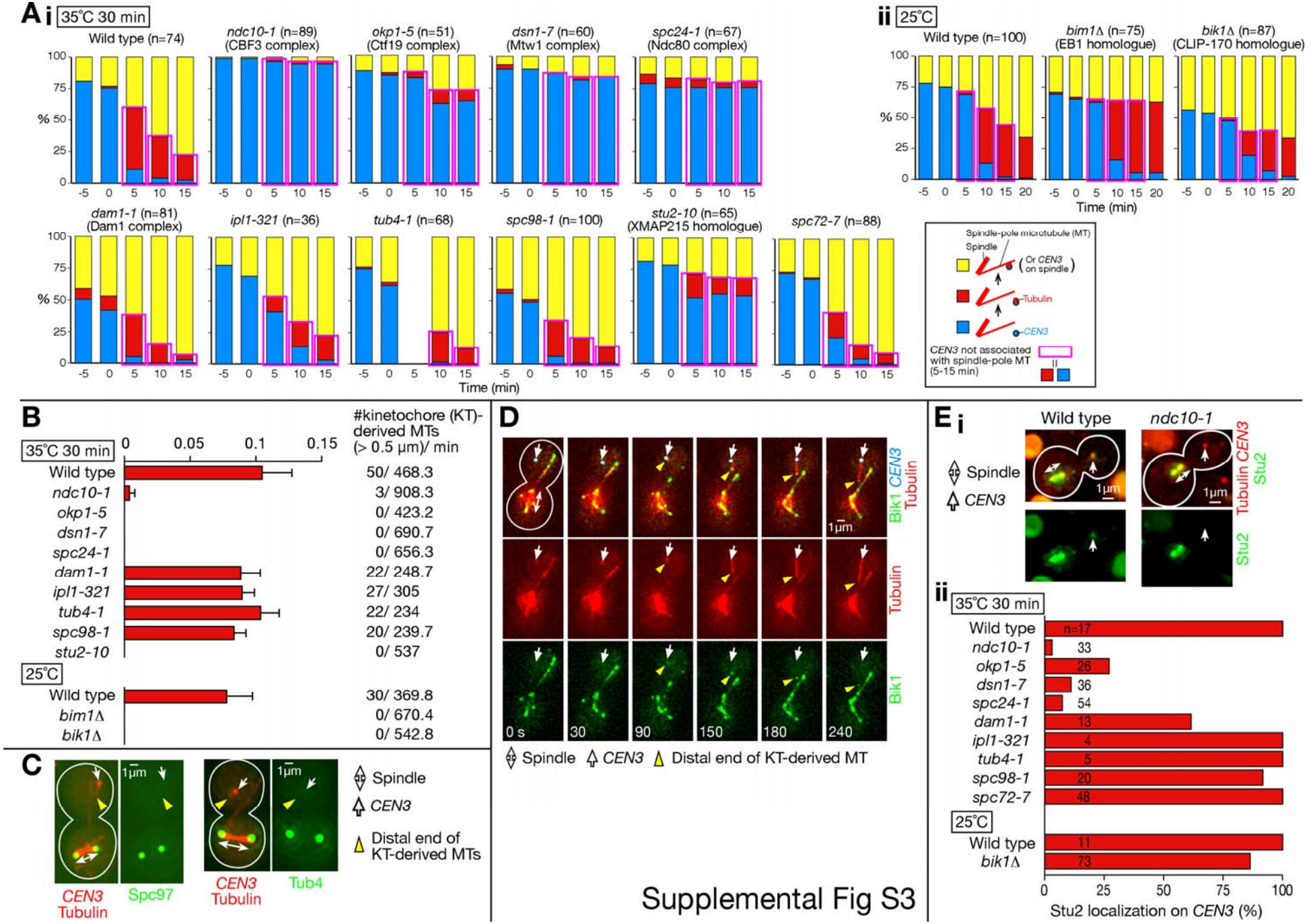
A i
35°C 30 min
Wild type (n=74)
ndc10-1 (n=89) (CBF3 complex)
okp1-5 (n=51) (Ctf19 complex)
dsn1-7 (n=60) (Mtw1 complex)
spc24-1 (n=67) (Ndc80 complex)
dam1-1 (n=81) (Dam1 complex)
ipl1-321 (n=36)
tub4-1 (n=68)
spc98-1 (n=100)
stu2-10 (n=65) (XMAP215 homologue)
spc72-7 (n=88)
% 100 75 50 25 0
-5 0 5 10 15
Time (min)
ii
25°C
Wild type (n=100)
bim1Δ (n=75) (EB1 homologue)
bik1Δ (n=87) (CLIP-170 homologue)
-5 0 5 10 15 20
Time (min)
Spindle-pole microtubule (MT)
Spindle
Or CEN3 on spindle
Tubulin
CEN3
CEN3 not associated with spindle-pole MT (5-15 min)
B
#kinetochore (KT)-derived MTs (> 0.5 µm)/ min
35°C 30 min
0 0.05 0.1 0.15
Wild type 50/ 468.3
ndc10-1 3/ 908.3
okp1-5 0/ 423.2
dsn1-7 0/ 690.7
spc24-1 0/ 656.3
dam1-1 22/ 248.7
ipl1-321 27/ 305
tub4-1 22/ 234
spc98-1 20/ 239.7
stu2-10 0/ 537
25°C
Wild type 30/ 369.8
bim1Δ 0/ 670.4
bik1Δ 0/ 542.8
C
1µm
CEN3 Tubulin
Spc97
CEN3 Tubulin
Tub4
Spindle
CEN3
Distal end of KT-derived MTs
D
Bik1 CEN3 Tubulin
Tubulin
Bik1
0 s 30 90 150 180 240
Spindle CEN3 Distal end of KT-derived MT
E i
Wild type
ndc10-1
Spindle
CEN3
Tubulin CEN3 Stu2
Stu2
ii
35°C 30 min
Wild type n=17
ndc10-1 33
okp1-5 26
dsn1-7 36
spc24-1 54
dam1-1 13
ipl1-321 4
tub4-1 5
spc98-1 20
spc72-7 48
25°C
Wild type 11
bik1Δ 73
0 25 50 75 100
Stu2 localization on CEN3 (%)
Supplemental Fig S3

Figure S3 (associated with Figure 3).

(A) The appearance of tubulin signals at *CEN3* and time course of *CEN3* interaction with spindle-pole microtubules in mutants (associated with Figure 3A ii)

(i) Wild-type (T3828), *ndc10-1* (T4230), *okp1-5* (T7983), *dsn1-7* (T4293), *spc24-1* (T4231), *dam1-1* (T4232), *ipl1-321* (T4414), *tub4-1* (T4409), *spc98-1* (T4410), *stu2-10* (T4296) and *spc72-7* (T8075) cells with *PGAL-CEN3-tetOs TetR-3×CFP YFP-TUB1 PMET3-CDC20* were treated as in Fig 3B. YFP (tubulin) and CFP (*CEN3*) images were acquired at time points indicated. Time 0: transfer to glucose-containing medium. The results are presented as in Fig 3B (bottom). "Tubulin localization on KT" was scored "+" in Fig 3A ii when tubulin signals were observed (red bars) on the majority of *CEN3*, which was not yet associated with spindle-pole microtubules (magenta rectangles), at least one time point (5 min or later).

(ii) Wild-type (T3828), *bim1Δ* (T4315) and *bik1Δ* (T4318) cells with *PGAL-CEN3-tetOs TetR-3×CFP YFP-TUB1 PMET3-CDC20* were treated as in Fig 1B. Images were acquired and the results are presented as in A.

(B) Frequency of microtubule extension from *CEN3* in mutants (associated with Figure 3A iii)

Top: Wild-type (T3531), *ndc10-1* (T2832), *okp1-5* (T3375), *dsn1-7* (T3528), *spc24-1* (T2902), *dam1-1* (T2897), *ipl1-321* (T2863), *tub4-1* (T3996), *spc98-1* (T3999) and *stu2-10* (T2862) cells with *PGAL-CEN3-tetOs TetR-GFP YFP-TUB1 PMET3-CDC20* were treated as in Fig 1C, except that temperature was raised to 35 °C, 30 min before cells were suspended in synthetic complete medium containing glucose and methionine. YFP (tubulin) and GFP (*CEN3*) signals were acquired together every 20 sec for 25 min at 35 °C. Kinetochore (KT)-derived microtubules were scored when they were observed for 2 or more time points and their maximum length was > 0.5 μm. The scored number of microtubules during the total observation time (the sum of observation time in multiple cells) is shown on the right. Bottom: Wild-type (T3531), *bim1Δ* (T2839) and *bik1Δ* (T2840) cells with *PGAL-CEN3-tetOs TetR-GFP YFP-TUB1 PMET3-CDC20* were treated as in Fig 1C. The number of microtubules extended from *CEN3* was scored as in the top.

(C) Components of the γ-tubulin complex localize at spindle poles, but not at *CEN3*

TUB4-3×GFP (T4045) and *SPC97-3×GFP* (T3906) cells with *PGAL-CEN3-tetOs TetR-3×CFP CFP-TUB1 PMET3-CDC20* were treated as in Fig 1C. YFP (*CEN3,* Tub1: red) and GFP (Tub4 or Spc97: green) images were acquired. Representative images are shown. *Results*: Tub4 and Spc97 signals were found with high intensity at spindle poles, but no signals were observed at *CEN3*.

(D) Localization of Bik1 at the plus ends of kinetochore-derived microtubuless, but not at kinetochores

T6718 cells (see Fig 5B) were treated as in Fig 1C. mCherry (Bik1; green), YFP (tubulin; red), and CFP (*CEN3*; blue) images were acquired every 30 sec (time 0; arbitrary). See also Movie S3.

(E) Stu2 localization at *CEN3* in mutants (associated with Figure 3A iv)

Wild-type (T3680), *ndc10-1* (T4480), *okp1-5* (T4486), *dsn1-7* (T4487), *spc24-1* (T4482), *dam1-1* (T4503), *ipl1-321* (T4011), *tub4-1* (T5407), *spc98-1* (T5409), *spc72-7* (T8123) and *bik1Δ* (T5541) cells with *PGAL-CEN3-tetOs TetR-3×CFP CFP-TUB1 STU2-3×GFP PMET3-CDC20* were treated as in Fig 3B (35 °C) and Fig 1B (25 °C). GFP (Stu2) and CFP (*CEN3*, tubulin) images were acquired. (i) Representative images. (ii) Percentages of cells in which Stu2 signals were detected at *CEN3* that was not associated with spindle-pole microtubules. When Stu2 signals were found in <15, 15-30, >60% of cells, the results were summarized as '-', 'decrease' and '+' of Stu2 signals, respectively, in Fig 3A iv.

Note. Spc72, which shows a limited homology to TACC proteins, is not involved in the generation of microtubules at kinetochores.

At centrosomes in metazoan cells, Stu2 orthologues are associated with TACC-family proteins: they cooperate to facilitate microtubule nucleation (Peset and Vernos, 2008). Similarly Spc72, which shows a limited homology to TACC proteins (Tien et al., 2004), binds Stu2 and cooperates for microtubule nucleation at SPBs in budding yeast (Chen et al., 1998; Usui et al., 2003). We therefore tested a possible role of Spc72 in generating microtubules at kinetochores, using the centromere reactivation assay. In *spc72-7* mutants (Knop and Schiebel, 1998), microtubule/tubulin signals were not reduced at kinetochores (Fig S3A), microtubules extended similarly to a wild-type control (data not shown) and Stu2 localized at kinetcohores similarly to a wild-type control (Fig S3E). Moreover Spc72 protein was not detected at kinetochores while its bright signals were detected at spindle poles (data not shown). Thus, it is unlikely that Spc72 is involved in microtubule generation at kinetochores.

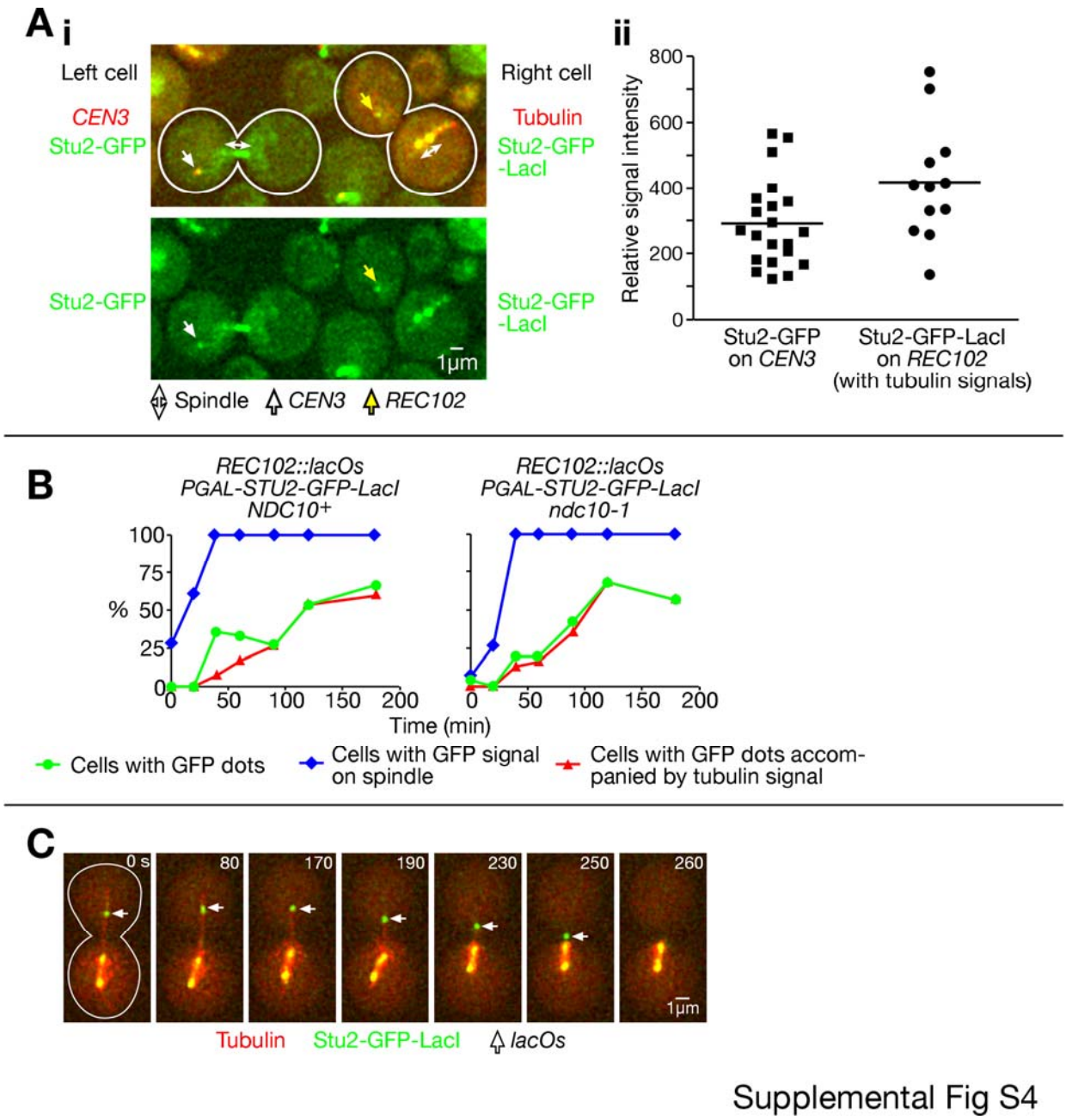

Figure S4, (associated with Figure 4).

(A) Comparison of the intensity of Stu2-GFP signals at *CEN3* and at the Stu2 tethered site

PGAL-CEN3-tetOs TetR-3xCFP STU2-GFP PMET3-CDC20 cells (T5477) were treated as in Fig 1B. After 10 min incubation with medium containing glucose and methionine, cells were fixed with paraformaldehyde. Meanwhile *PGALS-STU2-GFP-LacI REC102::lacOs CFP-TUB1 PMET3-CDC20* (T4837) cells were treated as in Fig 4B. After 60 min incubation with medium containing galactose and methionine, cells were fixed with paraformaldehyde. The two fixed samples were mixed, and then GFP (Stu2; green) and CFP (*CEN3,* tubulin; red) images were acquired.

(i) Images of representative T5477 and T4837 cells (left and right, respectively). Two kinds of cells were distinguished by the presence CFP signals for *CEN3* or the spindle. Scale bar represents 1 μm.

(ii) The intensity of Stu2-GFP signals at the subsets of *CEN3* (T5477) and *REC102* (T4837), on which tubulin signals were detected. To obtain these results six microscopy fields were analyzed, and there were no significant differences in the Stu2-GFP signal intensity of each strain between microscopy fields. Thick lines indicate mean values.

Results: The average accumulation level of Stu2 at its tethered site was higher than that at centromeres. Nonetheless several cells showed similar Stu2 signal intensity at the tethered site to that of centromeres, but still were associated with tubulin signals.

(B) Tubulin signals at the Stu2-tethered site are found in an *ndc10-1* mutant, as in wild-type control

NDC10^{+} (wild type *NDC10*$^{+}$; T4689) and *ndc10-1* (T5464) cells with *REC102::lacOs* P_{GAL}*-STU2-GFP-LacI CFP-TUB1* P_{MET3}*-CDC20* were treated as in Fig 4B, except that the temperature was raised to 35 °C, 30 min before galactose was added to the medium. Previous data suggested that incubation at 35 °C for 30 min was sufficient to impair the kinetochore assembly in *ndc10-1* mutant (Tanaka et al., 2005). GFP (Stu2 fused with LacI) and CFP (tubulin) images were acquired. Percentages of cells for each category are shown in coloured lines.
Results: The percentage of cells, in which microtubule/ tubulin signals were found at the Stu2-tethered site, increased similarly between the two strains, suggesting that microtubule nucleation at the Stu2-tethered site does not require a kinetochore component Ndc10.

(C) Stu2-tethered sites interacted with spindle-pole microtubules and were transported towards a spindle pole in some cells

T4837 cells (see A) were treated as in Fig 4C. GFP and CFP images were acquired every 10 sec.
Results: In some cells (10%, 6/63), Stu2-tethered sites interacted with the lateral sides of spindle-pole microtubules. Similar results were obtained in the presence (this figure) and absence of a mild osmotic stress (data not shown). This behaviour of Stu2-tethered sites was reminiscent to the behaviour of authentic kinetochores, which initially interact with the lateral sides of spindle-pole microtubules, subsequently slide along them towards a spindle pole, then attach to the plus ends of spindle-pole microtubules (end-on attachment) and move further poleward as they shrink (Tanaka et al., 2007; Tanaka et al., 2005). However, in contrast to kinetochores, Stu2-tethered sites did not preferentially show sliding towards a spindle pole. Instead, Stu2-tethered sites were associated with the plus ends of spindle-pole microtubules (end-on attachment) and transported poleward (as shown in this figure), which was similar to the later stage of kinetochore transport towards a spindle pole (Tanaka et al., 2007). However, while the end-on attachment of kinetochores to spindle-pole microtubules were stable and detachment was very rare (Tanaka et al., 2007), Stu2-tethered sites often detached from the end of these microtubules (data not shown).

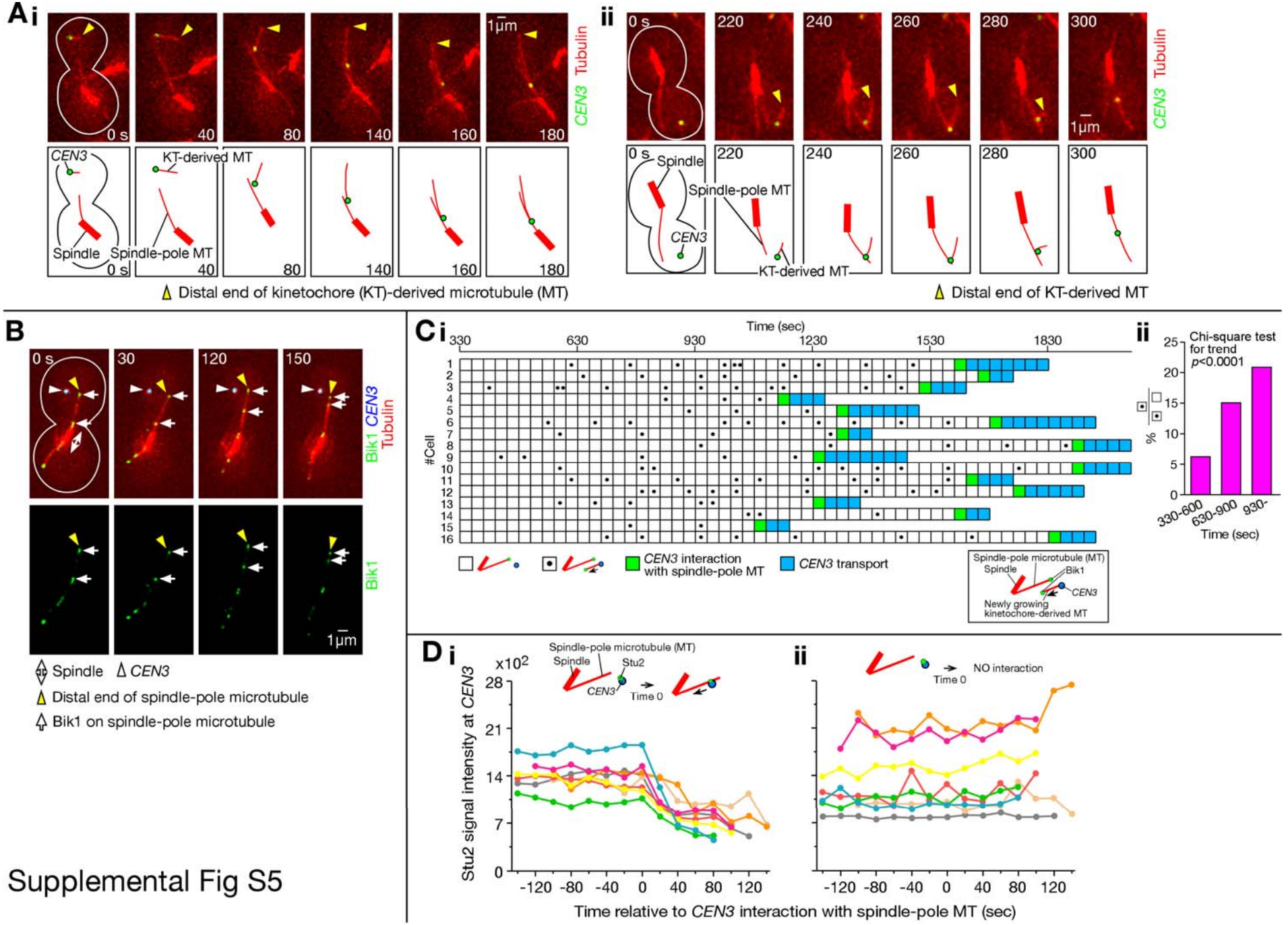

Supplemental Fig S5

Figure S5, (associated with Figure 5).

(A) In some cases, kinetochores are loaded onto the lateral surface of spindle-pole microtubules, which is followed by interaction between kinetochore-derived and spindle-pole microtubules

Experiments were carried out as in Fig 5A. In some cases, *CEN3*s interacted with spindle-pole microtubules first, followed by the association between kinetochore-derived and spindle-pole microtubules in a parallel (i) or anti-parallel manner (ii). Scale bar: 1 μm.

(**B) New growth of microtubules from a spindle pole is discerned even if they overlapped with microtubules that have extended earlier from the same spindle pole**

T6718 (see Fig S2) cells were treated as in Fig 1C. To discern overlapping spindle-pole microtubules, Bik1 was visualized with mCherry at the plus ends of growing microtubules.

Results: New growth of a microtubule from a spindle pole was recognized even if they overlapped with a microtubule that extended earlier from the same spindle pole, as: 1) Bik1 moved along the microtubule that extended earlier, and 2) tubulin signals showed higher intensity along the region where the microtubules overlapped.

(C) Microtubules do not show new growth from *CEN3* after *CEN3* interaction with spindle-pole microtubules (supplemental to Fig 5B i)

T6718 (see Fig S2) cells were treated as in Fig 1C. Images were acquired as in Fig S3D.

(i) Data in individual cells, observed for Fig 5B i. Time of transfer to glucose-containing media was defined as time 0. The numbers of time intervals, represented by white boxes with and without the black dots, were 531 and 101, respectively (the first and second bars from top in Fig 5B i). The total number of time intervals, represented by green and blue boxes, was 80 (the third bar from the top in Fig 5B i). *Results:* New microtubule growth was not observed during the time intervals, represented by blue or green boxes.

(ii) Percentage of time intervals, during which microtubules were newly extended from *CEN3* (that were not yet associated with spindle-pole microtubules). *Results*: The increase of this percentage at later time points suggests that microtubules are generated more frequently when kinetochore interaction with spindle-pole microtubule is delayed: the same conclusion has been also obtained in a normal S phase (see Fig 6C).

(**D) The amount of Stu2 at *CEN3* decreases soon after *CEN3* is loaded onto the surface of spindle-pole microtubules (supplemental to Fig 5B ii)**

Experiments were carried out and data were analyzed as in Fig 5B ii. (i) The quantified intensity of Stu2 signals at *CEN3* in 8 individual cells, where *CEN3* interacted with spindle-pole microtubules and no rescue occurred for these microtubules. Time is shown relative to the *CEN3* encounter with spindle-pole microtubules. (ii) As a control (shown in the same colour as [i]) for each cell in (i), Stu2 intensity was measured at the same time points in a neighbouring cell in the same microscope field, in which *CEN3* did not interact with spindle-pole microtubules. By collecting controls in this way, we could avoid possible bias due to photo-bleaching and possible variance in the Stu2 signal intensity between different microscopy fields.

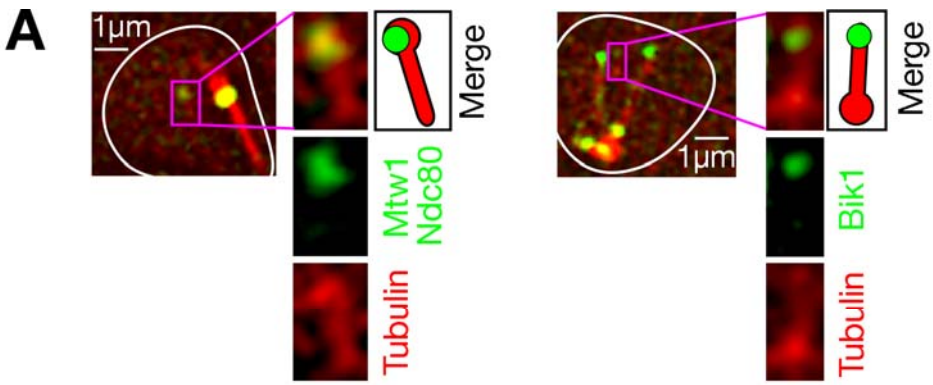

	Tubulin		
Mtw1 Ndc80	9/ 12	0/ 12	3/ 12
Bik1	0/ 7	6/ 7	1/ 7

p=0.0004

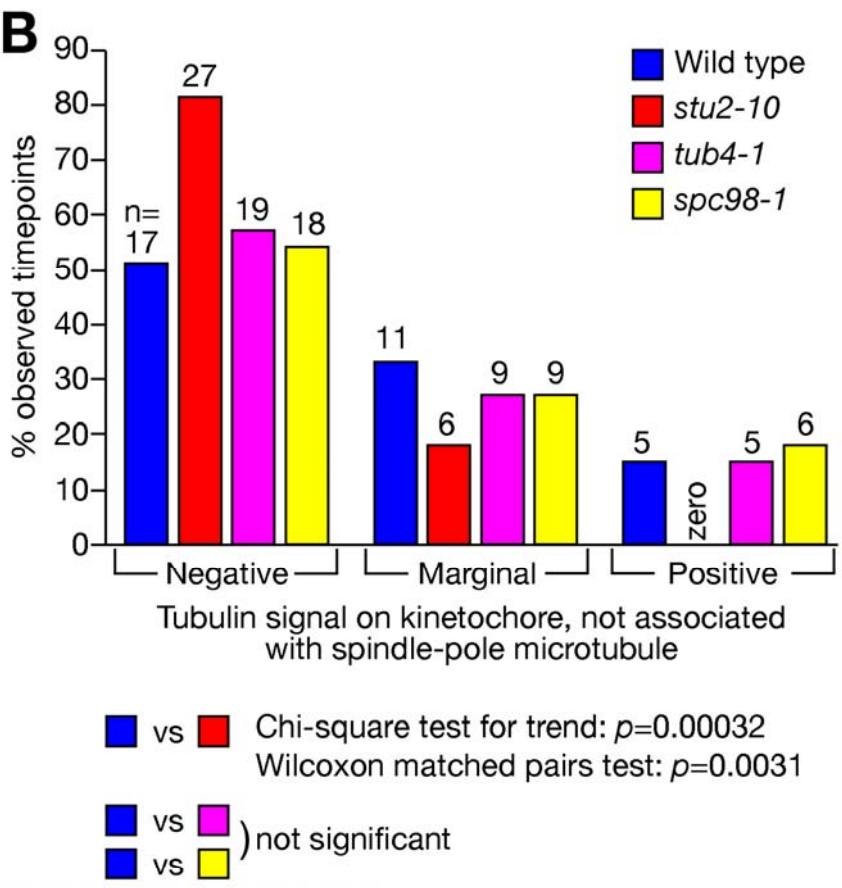

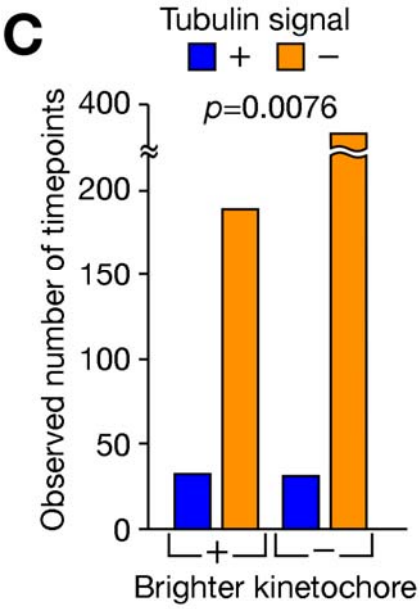

Supplemental Fig S6

Figure S6, (associated with Figure 6).

(A) Kinetochore-derived microtubules have their plus ends distal to kinetochores in a physiological condition

We investigated the polarity of microtubules generated at kinetochores during normal S phase (which overlaps with mitosis; Kitamura et al., 2007). *MTW1-4×mCherry NDC80-4×mCherry GFP-TUB1* (T8179) and *BIK1-4×mCherry GFP-TUB1* (T7972) cells were treated as in Fig 1A. mCherry (kinetochores or Bik1; green) and GFP (tubulin; red) images were acquired as in Fig 1A.

Top: Representative images. Rectangles (magenta; magnified at right) show microtubules generated at kinetochores that were not yet associated with spindle-pole microtubules.

Bottom: Scored localization patterns of Mtw1/Ndc80 (authentic kinetochore components) and Bik1 (a +TIP protein that localizes at the plus ends of growing microtubules).

Results: Tubulin often showed globular signals co-localizing at kinetochores (as also found in Fig 1B iii left and Fig S1B i), from which rod-like tubulin signal extended distal to kinetochores. The globular signals may correspond to unpolymerized tubulins or very short additional microtubules at kinetochores. Crucially, in most cases, Bik1 localized distal to the globular tubulin signals (at the end of rod-like signals); i.e. Bik1 localized at the microtubules ends distal to kinetochores. The results suggest that kinetochore-derived microtubules have their plus ends distal to kinetochores in normal S phase.

(B) *stu2-10* mutant cells, but not *tub4-1* or *spc98-1* mutants, show reduction in microtubule/ tubulin signals at kinetochores in a physiological condition

Wild-type control (T7199), *stu2-10* (T7057), *tub4-1* (T8327) and *spc98-1* (T8331) cells with *MTW1-4×mCherry NDC80-4×mCherry YFP-TUB1* were treated as in Fig 1A, except that temperature for cell culture was shifted to 35 °C when α factor was washed out. Images were acquired at 35 °C from 20 min after washout of α factor. mCherry (kinetochores) and YFP (tubulin) images were collected every 10 sec for 10 min. Percentage of time points (out of all time points observed in 8 cells), during which kinetochores were detected but not yet associated with spindle-pole microtubules, with positive, marginal or negative tubulin signals at kinetochores. See more detail in supplemental experimental procedures.

(C) Microtubule/tubulin signals are found more frequently at kinetochores with brighter signals

Using the data set shown in Fig 6A, the numbers of time points, at which tubulin signals (cyan box in Fig 6A) were present or absent at kinetochores, are shown by blue and orange bars, respectively, in correlation with the presence and absence of brighter kinetochore signals (orange dots in Fig 6A).

SUPPLEMENTAL EXPERIMENTAL PROCEDURES

Yeast genetics and molecular biology

The background of yeast strains (W303) and methods for yeast culture and α-factor treatment were as described previously (Amberg et al., 2005; Tanaka et al., 2007). Cells were cultured at 25 ºC in YP medium containing glucose, unless otherwise stated. Constructs of *PGAL-CEN3-tetOs* (Tanaka et al., 2005), *TetR-3×CFP* (Bressan et al., 2004), *PMET3-CDC20* (Uhlmann et al., 2000), *TetR-GFP* (Michaelis et al., 1997) and *REC102-lacOs* (Straight et al., 1996; Sullivan et al., 2004) were as described previously. Temperature-sensitive mutants *ndc10-1* (Goh and Kilmartin, 1993]), *okp1-5* (Ortiz et al., 1999), *dsn1-7* (Nekrasov et al., 2003), *spc24-1* (Wigge and Kilmartin, 2001), *dam1-1* (Cheeseman et al., 2001]), *ipl1-321* (Biggins et al., 1999), *tub4-1* (Spang et al., 1996), *spc98-1* (Geissler et al., 1996), *stu2-10* (Severin et al., 2001) were as described previously. To make *bim1Δ*, *bik1Δ* and *kar3Δ*, whole open reading frames of the relevant genes were replaced with antibiotic-resistance genes, using a one-step PCR method (Amberg et al., 2005). Yeast genes were tagged at their C-termini at their original gene loci by a one-step PCR method (Maekawa et al., 2003; Tanaka et al., 2005), using 3×GFP-KanMX6 (pSM1023; Maekawa et al., 2003) and 4×mCherry-NatMX6 (pT909) cassettes as PCR templates, unless otherwise stated. pT909 was constructed by multiplying the *mCherry* gene in pKS391 (Snaith et al., 2005). *CFP-TUB1* (Janke et al., 2002) and *YFP-TUB1* (pDH20, obtained from Yeast Resource Centre, Seattle, USA) plasmids were integrated at auxotroph marker loci. Strains with the tagged genes grew normally at temperatures used in this study.
To construct *TEL15R-tetOs*, 1198-bp genomic DNA fragment between *YOR387C* and *FDH1* (close to the right telomere of chromosome XV) was cloned into a plasmid carrying a hygromycin-resistance gene and an array of *tet* operators (112 copies); this plasmid (pT548) was cut with *Kpn*I within the genomic DNA fragment and integrated at this locus. To construct *TEL15L-tetOs*, 1369-bp genomic DNA fragment between *YOL159C-A* and *YOL159C* (close to the left telomere of chromosome XV) was cloned into a plasmid carrying a clonNAT-resistance gene and an array of *tet* operators (112 copies); this plasmid (pT543) was cut with *Nhe*I within the genomic DNA fragment and integrated at this locus. To construct *PGALS-GFP-LacI* and *PGALS-STU2-GFP-LacI* alleles, the *GALS* promoter (Mumberg et al., 1994) was subcloned into pAFS135 (pRS303-GFP12-LacI; Straight et al., 1998) at *Xho*I site (pT776). Subsequently *STU2* coding sequence was subcloned into pT776 at *Xho*I site (pT780). pT776 and pT780 were then cut with *Nhe*I and integrated at *HIS3* locus.

Live-cell imaging

The procedures for time-lapse fluorescence microscopy were described previously (Kitamura et al., 2007; Tanaka et al., 2007). Time-lapse images were collected at 25 ºC (ambient temperature) unless otherwise stated. For image acquisition, we used a DeltaVision RT microscope (Applied Precision), UPlanSApo 100× objective lens (Olympus; NA 1.40), a CoolSnap HQ CCD camera (Photometrics) and SoftWoRx software (Applied Precision). We acquired 5-9 (0.7 mm apart) z-sections, which were subsequently deconvoluted and analyzed with SoftWoRx and Volocity (Improvision) software. For figures, z stacks were projected to two-dimensional images. GFP signals were discriminated from YFP, using the JP3 filter set (Chroma). CFP, YFP (or GFP) and mCherry signals were discriminated with the 89006 ET filter set (Chroma). GFP and YFP signals were acquired together, using the YFP channel of the 89006 ET filter set.

Electron tomography

Samples were processed and analyzed as described previously (Hoog et al., 2007) with minor modifications. From 10 ml culture (OD=0.6), yeast cells were collected on polycarbonate filters (Millipore) using vacuum filtration, transferred to gold-plated flat specimen carriers and frozen by using the EM PACT2 high-pressure freezing machine (Leica Microsystems). The samples were then freeze-substituted at -90°C for 2 days in 0.1% OsO4, 0.1% glutaraldehyde and 0.2% uranyl acetate in acetone using the EM-AFS1 device (Leica Microsystems). Then the samples were gradually warmed up to -45 ºC and embedded in Lowicryl resin (HM20), which was polymerized under a UV lamp. Serial thin sections (280-300 nm thick) were cut using a Reichert Ultracut-E microtome (Leica Microsystems) and collected on Formvar-coated nickel grids. Sections were poststained with 4% uranyl acetate in 70% methanol for 4 min and with lead citrate for 1 min. Digital images were taken at 300kV from -60º to +60º tilt with 1º increment on a Tecnai TF30 electron microscope equipped with a Eagle 4K CCD camera (FEI: pixel size 1.18 nm at ×20,000 magnification). Tomograms were then generated by R-weighted back projection, modelled and analyzed using IMOD software (Kremer et al., 1996).

In Fig S1E, the diameter of spindle-pole microtubules was 18 nm. The smaller diameter of these microtubules than the standard 25 nm is probably due to sample processing for electron microscopy. The diameter of the presumable short MT in Fig S1E iii was very similar to that of spindle-pole MTs observed in the same cell.

Analyzing dynamics of kinetochores, microtubules and associated proteins

To evaluate the length of MTs and position of centromeres, we took account of the distance along the z-axis as well as distance on each z plane. The rate of microtubule growth and shrinkage was evaluated only for approximate linear changes (R^2

>0.85 in linear regression analyses) of microtubule length of more than 2 μm.

Statistical analyses were carried out with the Fisher's exact test (Fig 5B i, S6C), a paired *t*-test (Fig 5B ii; by comparing with an individual control), a chi-square test for trend (Fig 6C, S1C ii, S5C ii, S6B) or a log-rank test for survival curves (Fig 6E), an unpaired *t*-test (Fig S1C i), chi-square test (Fig S6A) or a Wilcoxon matched pairs test (Fig S6B), using the Prism (Graph pad) software. All *p* values are two-tailed. All error bars in figures represent SEM.

To visualize tubulins and MTs in Fig 1A and other figures, the *YFP-TUB1* construct was integrated in the genome (e.g. at *trp1* locus) of yeast cells that have the original *TUB1* (non-tagged) at its original locus. The integration of *YFP-TUB1* may have increased the total amount of Tub1 in cells and kinetochore-associated microtubule/tubulin signals might have been due to overexpression of Tub1. To address this possibility, cells with and without *YFP-TUB1* were analyzed using Western blotting with an anti-tubulin antibody (data not shown). The ratio of YFP-Tub1 and Tub1 amount was approximately 1: 5 and the total Tub1 expression level (YFP-Tub1 plus Tub1) was similar in the presence and absence of the extra *YFP-TUB1* copy, which is consistent with previous reports (Burke et al., 1989; Rusan et al., 2001). Therefore the appearance of kinetochore-associated microtubule/tubulin signals was not due to tubulin overexpression.

As shown in Fig 1C and other figures, microtubules extended for greater lengths from reactivated *CEN3* when cells were exposed to a mild osmotic stress. This was originally found when we fortuitously added 1/10 volume of concentrated glucose (20%) to culture medium after removing galactose to reactivate *CEN3*, instead of replacing galactose-containing culture medium with one containing 2% pre-diluted glucose as we usually do. This seemed to be due to osmotic stress, as it also happened when 1/10 volume of 1 M sorbitol was added immediately after replacement of galactose-containing medium with 2%, pre-diluted glucose-containing medium. In these conditions, spindle-pole microtubules did not change their dynamics (growth and shrinkage rates) significantly (Fig S1C i). If a higher-concentration of sorbitol (1/10 volume of 2 M) was added, polymerization and depolymerization of spindle-pole microtubules, as well as the extension of microtubules from *CEN3*, were halted for up to 12 min. This is consistent with a recent report that severe osmotic stress (addition of 1/2 volume of 2.4 M sorbitol) causes a cessation of microtubule dynamics (Robertson and Hagan, 2008). It is still unclear how a 'mild' osmotic stress facilitated generation of longer microtubules from *CEN3*. Nonetheless, treatment of cells with a mild osmotic stress gave us a useful means to make long *CEN3*-derived microtubules and observe their behaviour.

In Fig S1D, *PGAL-CEN3-tetOs TetR-3×CFP GFP-TUB1 PMET3-CDC20* cells (T6721) were treated as in Fig 1B and mixed with *CSE4-GFP* cells (T6799). Subsequently GFP (tubulin, Cse4) and CFP (*CEN3*) images were acquired. Separately, *GFP-TUB1 MTW1-4×mCherry NDC80-4×mCherry* cells (T6298) were mixed with *CSE4-GFP* cells (T6799). Then GFP (tubulin, Cse4) and mCherry (Mtw1 Ndc80) images were acquired. In T6721 cells, we focused on *CEN3*s that had been reactivated but not yet associated with spindle-pole microtubules. In T6298 cells, we found and focused on kinetochores, which had been reassembled away from a spindle pole during S phase but not yet associated with spindle-pole microtubules. At these *CEN3*s and kinetochores, the numbers of associated GFP-Tub1 and total Tub1 molecules, as well as the total length of associated microtubules were estimated as follows. We first quantified GFP signals (Tub1) at *CEN3*/kinetochores in T6721 and T6298 cells and compared them with GFP signals (Cse4) at a spindle pole in telophase of T6799 cells within the same microscopy field. Cse4 is a histone H3 variant at a centromere and 32 molecules (2 per centromere; Furuyama and Biggins, 2007) should be present close to a single spindle pole where 16 centromeres are clustered). From this comparison, we estimated how many GFP-Tub1 molecules were present at each kinetochore (as in Joglekar et al., 2006). Next we quantified the intensity of GFP-Tub1 signals along a single spindle-pole microtubule (which was found and confirmed as described in Tanaka et al., 2005) and estimated how many GFP-Tub1 molecules are contained along 1 μm of a single nuclear microtubule. We calculated how many Tub1 molecules should be present along 1 μm of the microtubule, and estimated that 6.9 % of the total Tub1 molecules are GFP-tagged. Finally, assuming that all *CEN3*/kinetochore-associated Tub1 molecules belong to either single or multiple short microtubules, and that the ratio of GFP-tagged Tub1 molecules to the total Tub1 molecules is the same at *CEN3*/kinetochores as along a spindle-pole microtubule, we estimated the total length of microtubules associated with each *CEN3*/kinetochore. We predicted that, if microtubules were longer than approximately 300 nm, their signals would show extended shapes (e.g. Fig S1B). Therefore, when the total length of *CEN3*-associated microtubules was longer than 300 nm but GFP-Tub1 signals did not show extension matching this length, *CEN3*/kinetochores were probably associated with multiple short microtubules.

In Fig 3A i, the extension of spindle-pole microtubules in the nucleus was scored as follows. Wild-type (T3270), *ndc10-1* (T3446), *okp1-5* (T3429), *dsn1-7* (T3392), *spc24-1* (T3274), *dam1-1* (T2897), *ipl1-321* (T2863), *tub4-1* (T5426), *spc98-1* (T5428), *stu2-10* (T3390), *bim1Δ* (T3410), and *bik1Δ* (T3514) cells with *PGAL-CEN3-tetOs TetR-GFP YFP-TUB1 NIC96-YFP KIP2-3GFP PMET3-CDC20* (except for T2897 and T2863, where *NIC96-YFP* and *KIP2-3GFP* were not present, and for T3514 where *KIP2-3GFP* was not present) were treated as in Fig 1B, but cultures were shifted to 35˚C, 30 min before transfer to glucose-containing medium (except for *bim1Δ* and *bik1Δ* cells and their control wild-type, where temperature was maintained at 25˚C). Subsequently, YFP (Tubulin and Nic96) and GFP (*CEN3* and Kip2) time-lapse images were acquired every 10 sec for 30 min at 35˚C (25˚C

for *bim1Δ* and *bik1Δ*). Using Nic96 signals (visualizing the nuclear envelope) and Kip2 signals (visualizing the plus ends of cytoplasmic microtubules), nuclear and cytoplasmic microtubules were distinguished (Tanaka et al., 2005). When *NIC96-YFP* and *KIP2-3GFP* were not present, nuclear microtubules were discerned by enhancing *TetR-GFP* signals that are present in the nucleus (TetR-GFP had a nuclear localization signal) but unbound to *tetOs*. These two methods gave almost identical results in 'wild-type' cells (data not shown). Because the extension of individual microtubules from spindle poles is generally observed more frequently with a monopolar spindle (for example, in *stu1-5* mutant: see supplementary note 5 in Tanaka et al., 2005) than with a bipolar spindle (in which, many spindle-pole microtubules inter-digitate in the middle of the spindle and not recognized as individual microtubules), the results of *tub4-1* and *spc98-1* cells, largely showing monopolar spindles, were not included for comparison in the table.
Also note that a part of the results in Fig 3A i, have been already published in (Tanaka et al., 2005).

In Fig 3B, tubulin YFP signals at CFP-labeled *CEN3* were scored negative when their integral signal intensity (from Voxel with the default setting of Volocity), colocalizing with the *CEN3*-CFP signal, was ≤ 95 and positive for > 95. In Fig 3C, the intensity of integral Mtw1/Ndc80 GFP signals, which colocalize with the *CEN3*-CFP signal, was scored as negative for ≤ 130 and positive for > 130.

In Fig 5B i, the extension of MTs were counted only when they were observed for two or more consecutive time points and their maximum length was > 0.5 μm.

In Fig 6A, kinetochore assembly was scored when its integral signal intensity was > 80 and the signal moved towards a spindle pole at later time points; brighter kinetochores were scored when its integral signal intensity was > 132. Tubulin signals at kinetochores were scored positive when their intensity was > 107.

From the regression curve obtained in Fig 6D, we reasoned that some events of kinetochore reassembly and subsequent interaction with spindle-pole MTs were not recognized in Fig 6A when the time interval between the two was very short. The addition of hypothetical 18 and 15 events of kinetochore assembly, followed by kinetochore interaction with spindle MTs at 10 and 20 sec, respectively, gave the best fit to the regression curve in Fig 6D, and they were therefore taken into consideration when black dots were plotted in Fig 6E and to plot the number of free kinetochores at time 0 in Fig 6D. Because in these hypothetical events the assembled kinetochores rapidly interacted with spindle-pole MTs, we assumed that "brighter kinetochore signal" and "tubulin signal at kinetcohore" were not positive.

In Fig 6E i and ii, we evaluated the effect of kinetochore-associated microtubules /tubulins on efficient kinetochore interaction with spindle–pole microtubules. However this effect is probably under-estimated by the method used there, because of the following reason. To estimate this effect, we plotted how quickly the percentage of free kinetochores decreased after tubulin signals had first appeared at kinetochores (blue and magenta curves in Fig 6 E i, ii). We then compared these curves with the control curve (black curves) showing the decrease of free kinetochores since their reassembly had been detected, including all 75 samples shown in Fig 6A. One might think that, a more precise estimation of the above effect could be obtained by excluding the samples in Fig 6A, where tubulin signals appeared at kinetochores, from the control curve. Unfortunately this did not prove a good option because this exclusion would lead to a bias towards samples that showed rapid kinetochore interaction with spindle-pole microtubules, because tubulin signals preferentially appeared at kinetochores when this interaction was delayed (see Fig 6C i, ii). It was therefore inevitable to use all samples in order to avoid such a bias in making a control curve. Because the control included both samples where tubulin signals did and did not appear at kinetochores, we probably underestimated the effect of kinetochore-associated microtubules/ tubulins in facilitating kinetochore interaction with spindle-pole microtubules. In both Fig 6 E i and ii, "time for 50%" was shorter, relative to the control curve. However, in a log-rank test for survival curves, the effect was significant (see *p* values) only when tubulin signals appeared at kinetochores at 2 or more consecutive time points. Nonetheless, because of this probable under-estimation, the tubulin-signal appearance may indeed have the effect even if they did not appear at consecutive time points.

In Fig S6B, kinetochore assembly was scored positive when its integral signal intensity (from Voxel with the default setting of Volocity) was >80. We noticed that it took longer time for kinetochore signals (since their appearance) to interact with spindle-pole microtubules in *stu2-10*, *tub4-1*, *spc98-1* mutant cells (actually, in the majority of *stu2-10* cells, the interaction did not happen during observation) than in wild-type control, due to the reduced number of spindle-pole microtubules (data not shown). On the other hand, tubulin signals appeared at kinetochores more frequently when kinetochore interaction with spindle microtubules was delayed (see Fig 6C i and ii). Therefore, if we had considered for scoring tubulin signals all the time points during which kinetochores were not associated with spindle pole microtubules in the mutant cells, this might have given a bias towards higher tubulin signals due to a delay in kinetochore interaction with spindle microtubules in these cells. We therefore scored tubulin signals at kinetochores by making 8 pairs between each mutant and wild-type cells in the order of the time length required for kinetochore interaction with spindle-pole microtubules (or, in *stu2-10* cells, the time length, during which kinetochores were observed without this interaction, until the end of the imaging): for example, a mutant cell, in which kinetochores were observed for the shortest time length without this interaction, was matched with the wild-type cell with the quickest

interaction, second with second, so on. In all pairs, mutant cells gave the same or a larger number of time points, in which kinetochores were not associated with spindle microtubules, than wild-type cells. We then scored tubulin signals only at the time points (since the appearance of kinetochore signals; relative to this appearance) in each mutant cell, at which kinetochores were not yet associated in the paired wild-type cell. The time points were also paired in this way between paired mutant and wild-type cells, in order to score tubulin signals between the paired time points using a Wilcoxon matched pairs test (used for comparison of paired non-parametric samples).

In addition to the above experiment, we also compared timing of kinetochore assembly in *stu2-10*, *tub4-1* and *spc98-1* mutant cells and wild-type control, after *CEN* detachment from microtubules upon *CEN* DNA replication. For this, we used cells with similar genotype to Fig S6B, but with CFP-labelled *CEN5*, treated cells as in Fig S6B and collected mCherry (kinetochores Mtw1/Ndc80), YFP (tubulin) and CFP (*CEN5*) images. Time from *CEN5* detachment (from spindle-pole microtubules) until Mtw1/Ndc80 reappearance at *CEN5* was similar between the 4 strains (data not shown). Thus, timing of kinetochore assembly in *stu2-10*, *tub4-1* and *spc98-1* mutants was similar to that in wild-type cells.

SUPPLEMENTAL REFERENCES

Amberg, D.C., Burke, D.J., and Strathern, J.N. (2005). Methods in yeast genetics (CSHL press).

Biggins, S., Severin, F.F., Bhalla, N., Sassoon, I., Hyman, A.A., and Murray, A.W. (1999). The conserved protein kinase Ipl1 regulates microtubule binding to kinetochores in budding yeast. Genes Dev *13*, 532-544.

Bressan, D.A., Vazquez, J., and Haber, J.E. (2004). Mating type-dependent constraints on the mobility of the left arm of yeast chromosome III. J Cell Biol *164*, 361-371.

Burke, D., Gasdaska, P., and Hartwell, L. (1989). Dominant effects of tubulin overexpression in Saccharomyces cerevisiae. Mol Cell Biol *9*, 1049-1059.

Cheeseman, I.M., Enquist-Newman, M., Muller-Reichert, T., Drubin, D.G., and Barnes, G. (2001). Mitotic spindle integrity and kinetochore function linked by the Duo1p/Dam1p complex. J Cell Biol *152*, 197-212.

Chen, X.P., Yin, H., and Huffaker, T.C. (1998). The yeast spindle pole body component Spc72p interacts with Stu2p and is required for proper microtubule assembly. J Cell Biol *141*, 1169-1179.

Furuyama, S., and Biggins, S. (2007). Centromere identity is specified by a single centromeric nucleosome in budding yeast. Proc Natl Acad Sci U S A *104*, 14706-14711.

Geissler, S., Pereira, G., Spang, A., Knop, M., Soues, S., Kilmartin, J., and Schiebel, E. (1996). The spindle pole body component Spc98p interacts with the gamma-tubulin-like Tub4p of Saccharomyces cerevisiae at the sites of microtubule attachment. EMBO J *15*, 3899-3911.

Goh, P.Y., and Kilmartin, J.V. (1993). NDC10: a gene involved in chromosome segregation in Saccharomyces cerevisiae. J Cell Biol *121*, 503-512.

Hoog, J.L., Schwartz, C., Noon, A.T., O'Toole, E.T., Mastronarde, D.N., McIntosh, J.R., and Antony, C. (2007). Organization of interphase microtubules in fission yeast analyzed by electron tomography. Dev Cell *12*, 349-361.

Janke, C., Ortiz, J., Tanaka, T.U., Lechner, J., and Schiebel, E. (2002). Four new subunits of the Dam1-Duo1 complex reveal novel functions in sister kinetochore biorientation. Embo J *21*, 181-193.

Joglekar, A.P., Bouck, D.C., Molk, J.N., Bloom, K.S., and Salmon, E.D. (2006). Molecular architecture of a kinetochore-microtubule attachment site. Nat Cell Biol *8*, 581-585.

Kitamura, E., Tanaka, K., Kitamura, Y., and Tanaka, T.U. (2007). Kinetochore microtubule interaction during S phase in Saccharomyces cerevisiae. Genes Dev *21*, 3319-3330.

Knop, M., and Schiebel, E. (1998). Receptors determine the cellular localization of a gamma-tubulin complex and thereby the site of microtubule formation. EMBO J *17*, 3952-3967.

Kremer, J.R., Mastronarde, D.N., and McIntosh, J.R. (1996). Computer visualization of three-dimensional image data using IMOD. J Struct Biol *116*, 71-76.

Maekawa, H., Usui, T., Knop, M., and Schiebel, E. (2003). Yeast Cdk1 translocates to the plus end of cytoplasmic microtubules to regulate bud cortex interactions. Embo J *22*, 438-449.

Michaelis, C., Ciosk, R., and Nasmyth, K. (1997). Cohesins: chromosomal proteins that prevent premature separation of sister chromatids. Cell *91*, 35-45.

Mumberg, D., Muller, R., and Funk, M. (1994). Regulatable promoters of Saccharomyces cerevisiae: comparison of transcriptional activity and their use for heterologous expression. Nucleic Acids Res *22*, 5767-5768.

Nekrasov, V.S., Smith, M.A., Peak-Chew, S., and Kilmartin, J.V. (2003). Interactions between centromere complexes in Saccharomyces cerevisiae. Mol Biol Cell *14*, 4931-4946.

O'Toole, E.T., Winey, M., and McIntosh, J.R. (1999). High-voltage electron tomography of spindle pole bodies and early mitotic spindles in the yeast Saccharomyces cerevisiae. Mol Biol Cell *10*, 2017-2031.

Ortiz, J., Stemmann, O., Rank, S., and Lechner, J. (1999). A putative protein complex consisting of Ctf19, Mcm21, and Okp1 represents a missing link in the budding yeast kinetochore. Genes Dev *13*, 1140-1155.

Peset, I., and Vernos, I. (2008). The TACC proteins: TACC-ling microtubule dynamics and centrosome function. Trends Cell Biol *18*, 379-388.

Robertson, A.M., and Hagan, I.M. (2008). Stress-regulated kinase pathways in the recovery of tip growth and microtubule dynamics following osmotic stress in S. pombe. J Cell Sci *121*, 4055-4068.

Rusan, N.M., Fagerstrom, C.J., Yvon, A.M., and Wadsworth, P. (2001). Cell cycle-dependent changes in microtubule dynamics in living cells expressing green fluorescent protein-alpha tubulin. Mol Biol Cell *12*, 971-980.

Severin, F., Habermann, B., Huffaker, T., and Hyman, T. (2001). Stu2 promotes mitotic spindle elongation in anaphase. J Cell Biol *153*, 435-442.

Snaith, H.A., Samejima, I., and Sawin, K.E. (2005). Multistep and multimode cortical anchoring of tea1p at cell tips in fission yeast. EMBO J *24*, 3690-3699.

Spang, A., Geissler, S., Grein, K., and Schiebel, E. (1996). gamma-Tubulin-like Tub4p of Saccharomyces cerevisiae is associated with the spindle pole body substructures that organize microtubules and is required for mitotic spindle formation. J Cell Biol *134*, 429-441.

Straight, A.F., Belmont, A.S., Robinett, C.C., and Murray, A.W. (1996). GFP tagging of budding yeast chromosomes reveals that protein-protein interactions can mediate sister chromatid cohesion. Curr Biol *6*, 1599-1608.

Straight, A.F., Sedat, J.W., and Murray, A.W. (1998). Time-lapse microscopy reveals unique roles for kinesins during anaphase in budding yeast. J Cell Biol *143*, 687-694.

Sullivan, M., Higuchi, T., Katis, V.L., and Uhlmann, F. (2004). Cdc14 phosphatase induces rDNA condensation and resolves cohesin-independent cohesion during budding yeast anaphase. Cell *117*, 471-482.

Tanaka, K., Kitamura, E., Kitamura, Y., and Tanaka, T.U. (2007). Molecular mechanisms of microtubule-dependent kinetochore transport toward spindle poles. J Cell Biol *178*, 269-281.

Tanaka, K., Mukae, N., Dewar, H., van Breugel, M., James, E.K., Prescott, A.R., Antony, C., and Tanaka, T.U. (2005). Molecular mechanisms of kinetochore capture by spindle microtubules. Nature *434*, 987-994.

Tien, A.C., Lin, M.H., Su, L.J., Hong, Y.R., Cheng, T.S., Lee, Y.C., Lin, W.J., Still, I.H., and Huang, C.Y. (2004). Identification of the substrates and interaction proteins of aurora kinases from a protein-protein interaction model. Mol Cell Proteomics *3*, 93-104.

Uhlmann, F., Wernic, D., Poupart, M.A., Koonin, E.V., and Nasmyth, K. (2000). Cleavage of cohesin by the CD clan protease separin triggers anaphase in yeast. Cell *103*, 375-386.

Usui, T., Maekawa, H., Pereira, G., and Schiebel, E. (2003). The XMAP215 homologue Stu2 at yeast spindle pole bodies regulates microtubule dynamics and anchorage. Embo J *22*, 4779-4793.

Wigge, P.A., and Kilmartin, J.V. (2001). The Ndc80p complex from Saccharomyces cerevisiae contains conserved centromere components and has a function in chromosome segregation. J Cell Biol *152*, 349-360.